


SCIENTIFIC REPORTS



OPEN

Consistent visuomotor adaptations and generalizations can be achieved through different rotations of robust motor modules

Cristiano De Marchis¹, Jacopo Di Somma^{1,2}, Magdalena Zych², Silvia Conforto¹ & Giacomo Severini² 

Humans can adapt their motor commands in response to alterations in the movement environment. This is achieved by tuning different motor primitives, generating adaptations that can be generalized also to relevant untrained scenarios. A theory of motor primitives has shown that natural movements can be described as combinations of muscle synergies. Previous studies have shown that motor adaptations are achieved by tuning the recruitment of robust synergy modules. Here we tested if: 1) different synergistic tunings can be achieved in response to the same perturbations applied with different orders of exposure; 2) different synergistic tunings can explain different patterns of generalization of adaptation. We found that exposing healthy individuals to two visuomotor rotation perturbations covering different parts of the same workspace in a different order resulted in different tunings of the activation of the same set of synergies. Nevertheless, these tunings resulted in the same net biomechanical adaptation patterns. We also show that the characteristics of the different tunings correlate with the presence and extent of generalization of adaptation to untrained portions of the workspace. Our results confirm synergies as invariant motor primitives whose recruitment is dynamically tuned during motor adaptations.

Complex movements can be easily adapted in response to discrepancies between the expected and actual sensorimotor outputs. This is achieved through the recalibration of the neural representation of the body and the environmental interaction dynamics that are thought to be stored in internal models that characterize both the forward and inverse dynamics of movement^{1–6}. Internal models can be adapted as a response to changes in the mapping between movement and its associated feedback or in response to perturbations modifying the dynamic characteristics of the movement in a relevant way⁷.

Several seminal studies have suggested that internal models are constituted by combinations of motor primitives^{8–12}, an observation that is corroborated by the fact that adaptation to specific perturbations can be generalized to untrained compatible contexts^{9–11,13–16}. These motor primitives are thought to explain the mapping between state variables such as limb position and movement velocities, into motor commands¹².

A conceptually correlated theory of motor primitives and movement modularity has been proposed and widely demonstrated in both animal models and humans, that is, the muscle synergies hypothesis^{17–20}. Muscle synergies are thought to be the functional building blocks of force production during natural movements. Studies employing stimulation^{21–24} and optogenetics^{25,26} techniques have individuated the presence of such modules in the spinal cord of rodents, frogs and primates. In humans, on top of the fertile literature describing muscle synergies during natural behaviors^{27–32}, studies on impaired individuals have demonstrated the solidity of this hypothesis in describing neurological conditions such as stroke^{33,34}.

As motor adaptations have been mainly studied, in humans, using computational models derived from metrics of biomechanical error, there is small evidence connecting the re-organization of the internal models that happens during adaptation with the supposed functional constituents of movement.

¹Department of Engineering, University of Roma TRE, via Vito Volterra 62, Rome, Italy. ²School of Electrical & Electronic Engineering, University College Dublin, Belfield, Dublin 4, Ireland. Correspondence and requests for materials should be addressed to G.S. (email: giacomo.severini@ucd.ie)

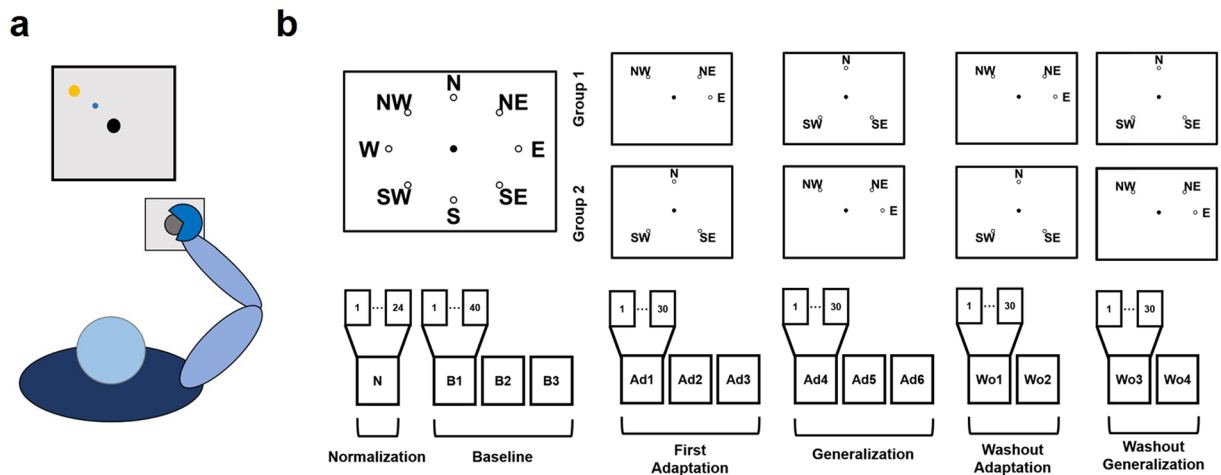


Figure 1. The experimental setup and protocol. Panel (a) presents a graphical representation of the task. Subjects kept their position consistent across all trials. The forearm was strapped to a support surface (not shown in the picture) and the hand was strapped to the manipulandum to avoid the use of the hand muscles during the task. Subjects were presented a virtual scene on a screen in front of them. During the whole experiment, subjects performed a total of 14 exercise blocks (b). The number of movements experienced in each block varied between 24 and 40. During the normalization (N) and baseline (B1–B3) blocks both groups of subjects experienced all 8 targets (3 repetitions of each target during normalization, 5 during baseline). During the adaptation (Ad1–Ad3) and generalization (Ad4–Ad6) blocks subjects experienced a limited target-set of 3 targets (NW, NE and E for target-set 1; N, SE and SW for target-set 2; each target was experienced 10 times in each block). Group1/Group2 experienced target-set 1/target-set 2 during adaptation and target-set 2/target-set 1 during generalization. A CW visuomotor rotation of 45° was applied during Ad1–Ad6. During the washout blocks (Wo1–Wo4) subjects experienced the same target-sets as in Ad1–Ad6, without the visual rotation.

Previous studies have suggested muscle synergies as potential physiological blocks of computationally-derived primitive-based models¹², but only in recent years muscle synergies analysis has been used to describe adaptive behaviors, including visuomotor adaptations during isometric reaching movements^{35–37}. In this latter scenario, studies have shown that muscle synergies are robust with respect to changes in the motor plan³⁶, and that adaptation to specific perturbations depends on how the perturbations map on the synergistic structure^{35,37}. As a case in point, it has been demonstrated that adaptation to a 45° visuomotor rotation is achieved by similarly rotating the activation maps of a set of fixed muscle synergies³⁶.

Nevertheless, if adaptation to visuomotor rotations is achieved by rotating the activation patterns of synergies of specific shape and workspace, either the synergies are rotated solidly and invariantly in response to consistent perturbations or, more likely, the patterns of rotation of each synergy depend on the spatial and temporal characteristics of the training. In such modular model, a visuomotor rotation that only affects a portion of the movement space is supposed to induce the rotation of only the subset of synergies active in that subspace, to an extent that depends on the effect of the perturbation on the synergistic workspace.

A dynamic synergistic model of adaptation like the one just described could explain adaptation-related phenomena such as generalization. Generalization of visuomotor rotations has been observed to depend on both the distance between the pre-adapted targets and the newly experienced ones³⁸ and the amount of angular rotation of the perturbation that needs to be generalized³⁹. In a muscle synergy-based representation, both phenomena could depend on which specific synergies have been rotated and how they have been rotated during the initial adaptation.

Herein we tested the hypotheses that the tuning of synergies recruitment that happens during adaptation to visuomotor rotations is not invariant but depends dynamically on the way in which the perturbations are experienced. We also tested the hypothesis that the characteristics of the tuning achieved through adaptation correlate with the presence and extent of generalization. To do so we investigated (1) if synergies always rotate in the same way when adapting to the same visuomotor rotations experienced in different parts of the workspace in different temporal orders and (2) if the way in which synergies are rotated during an adaptation exercise performed on a specific subspace correlates with generalizing behaviors observed in a subsequent adaptation exercise performed on a different subspace.

Results

Experimental Protocol. We designed a single experiment that could be used to test our initial hypotheses (Fig. 1). In the experiment, subjects trained to counteract a 45° clockwise (CW) rotation during isometric reaching movements. Subjects first experienced a series of baseline blocks (B1–B3) where they practiced reaching to eight different targets positioned in a compass-like configuration and at a distance equivalent to 15 N. After that, subjects trained to adapt six of the eight available targets to the CW rotation, divided in two target-sets of three targets each. The subjects experienced one of the two target-sets during three blocks of adaptation (Ad1/Ad3) and

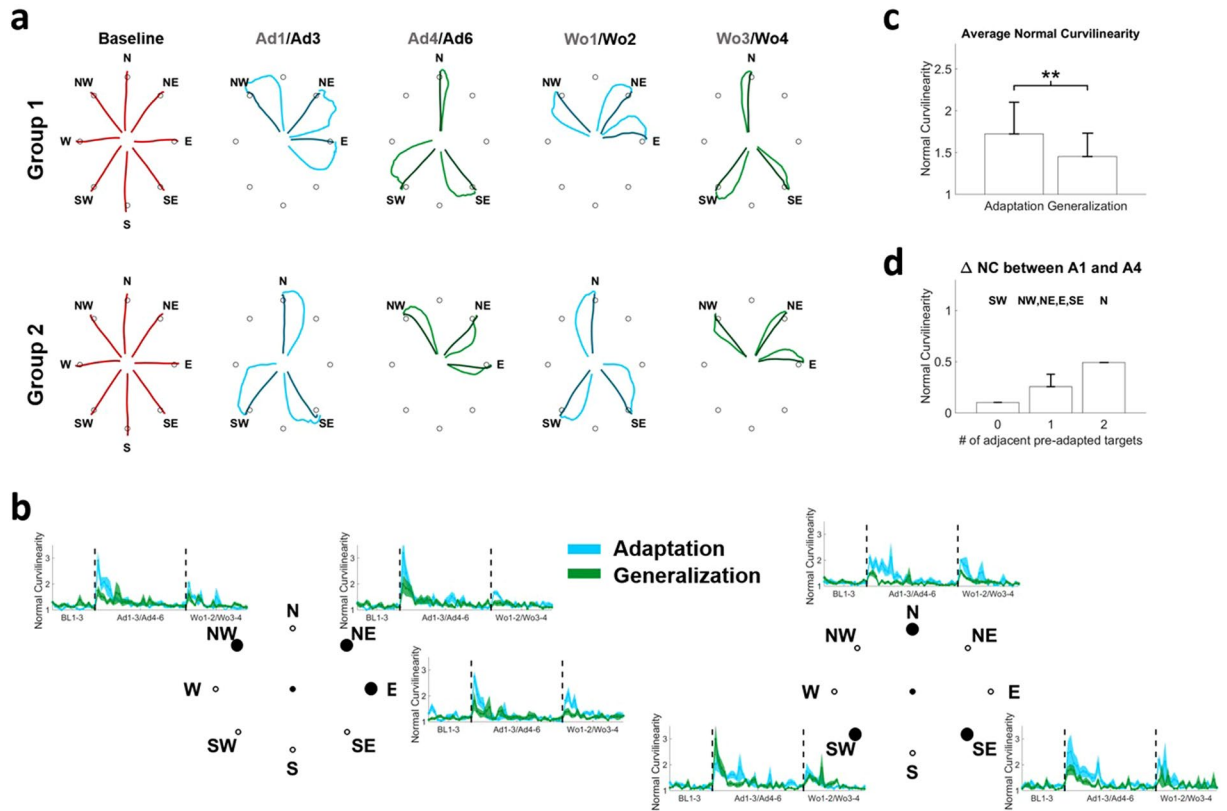


Figure 2. Adaptation and generalization in the biomechanics. Panel (a) presents the average trajectories observed at Baseline (red), Ad1/Ad3 (blue), Ad4/Ad6 (green), Wo1/Wo2 (blue) and Wo3/Wo4 (green). For each plot the lighter color presents the average of the first 2 movements in the first block listed on top (e.g. Ad1) and the darker color presents the average of the last 2 movement in the second block listed on top (e.g. Ad3). For baseline, the average of the last 5 movements of B3 is presented. For each target we observed an increase in movement curvilinearity at the onset of the perturbation (b) followed by an adaptation and a second increase when the perturbation is removed. Similar behaviors were observed during adaptation (light blue) and generalization (light green) although generalization was characterized by smaller initial deviations at the onset and offset of the perturbation for all targets with the exclusion of target SW. The average normal curvilinearity was significantly higher at the beginning of adaptation with respect of generalization across all targets (c). **denotes $p < 0.01$, using Mann-Whitney U test. Panel (d) shows the average values of generalization (calculated as the average difference in NC between Ad1 and Ad4 across the subjects) for the targets as a function of the number of pre-adapted adjacent targets.

the other one during three blocks of generalization (Ad4/Ad6). The subjects were divided in two groups: Group1 adapted target-set 1 (TS1 that included targets NW, NE and E) during the adaptation blocks and target-set 2 (TS2 that included targets N, SE and SW) during the generalization blocks, while Group2 adapted TS2 during the adaptation blocks and TS1 during the generalization blocks. After the generalization blocks subjects performed two sets of washout blocks (two blocks per set) where they first washed out the target-set adapted during the adaptation phase (Wo1/Wo2) and then that adapted during the generalization phase (Wo3/Wo4). TS1 and TS2 were designed so that one target-set would span only a limited part of the workspace (TS1, spanning a total of 135°) while the other one would present targets scattered through all the workspace (TS2). This choice was made under the hypothesis that training on a smaller subspace would lead to the rotation of a smaller sub-set of synergies with respect to a wider subspace, thus allowing to test the hypothesis of differential rotation. In addition, this choice of targets allows for different configurations between pre-adapted and generalized targets. Specifically, the two target-sets include: i) targets with no adjacent pre-adapted targets (SW, TS2); ii) targets with one pre-adapted target (NW, NE and E in TS1 and SE in TS2); iii) targets with both adjacent targets pre-adapted (N, TS2).

Adaptation and generalization in the biomechanics. The analysis of the force trajectories recorded during the experiments showed that: a) subjects were able to fully adapt to both target-sets regardless of whether they were presented during adaptation or generalization; b) the marked patterns of generalization that can be observed across the different targets are generally dependent on the distance between the generalized targets and the previously adapted ones. These results are presented in Fig. 2.

As expected, both groups presented an effect of the visual perturbation at the beginning of the adaptation period that was characterized by a CW-rotated initial trajectory followed by a compensatory movement (Fig. 2a). Subjects were able to quickly and fully adapt to this perturbation and were able to perform the movements with

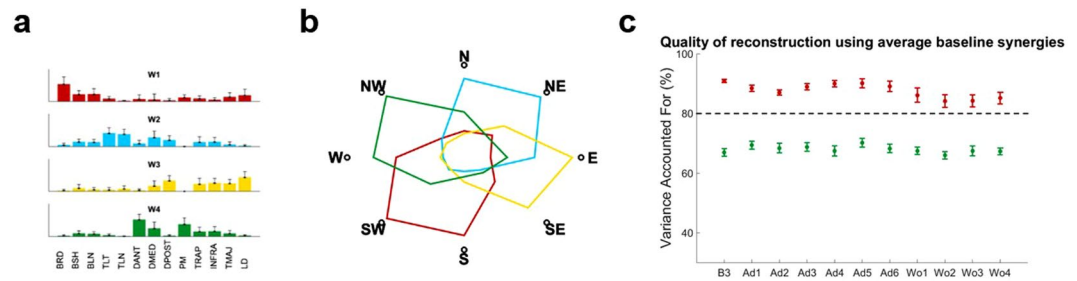


Figure 3. Muscle Synergies extracted at baseline. Four muscles synergies could well represent the whole dataset (a). The RMS values of the activation patterns of each synergy at each target were used to represent the spatial boundaries of each module in the workspace (b). The modules (a) extracted during B3 were used to estimate the activation patterns able to describe the movements in all the blocks. We found that the four original synergies were able to represent the data with acceptable median VAF (>80%) in each block (c). The VAF calculated for each block (red errorbars, indicating median and standard error) were significantly higher than the ones obtained using random modules (green errorbars). For each block statistical significance was estimated using Mann-Whitney U test and Bonferroni's correction.

straight trajectories by the end of the adaption period. At the beginning of the first generalization block, both groups presented smaller initial deviations that were again fully compensated. After the visual rotation was removed, subjects presented marked after-effects during the washout periods of the adaptation target-set and, to a lesser extent, of the generalization one. We analyzed the patterns of adaptation and generalization in terms of the Normal Curvilinearity (NC) metric that is calculated as the ratio between the length of the actual and ideal rectilinear trajectories. This metric was selected because, with respect to other metrics such as the initial angular error³⁶, it keeps into account both the initial angular error and potential compensatory movements. As preliminary observed, subjects presented values of NC close to 1 (equal to the ideal straight trajectory) during baseline (Fig. 2b). Once the visual perturbation was introduced (either during adaptation or generalization) the value of NC suddenly increased and was then reduced again close to 1 by the end of the last adaptation/generalization block (Ad3/Ad6). Once the perturbation was removed, subjects once again exhibited an increase in NC (indicating the presence of the after-effect) that was quickly washed out. For all targets, with the exclusion of SW, the NC values recorded during the first block (10 repetitions) of generalization were generally lower than the respective values during adaptation. For all targets both groups showed the same level of final adaptation/generalization in the last perturbed block (Ad3/Ad6). Similarly, after-effects were shown to be lower for generalization than for adaptation in the first washout block for all targets with the exclusion of SW. These results suggest a marked presence of generalization in our tests, characterized by smaller biomechanical errors at the beginning of the generalization period in targets close to the ones that were previously adapted. To confirm upon this point we compared, across all subjects, the average NC calculated for each target during the first adaptation and first generalization blocks, for all targets pooled together. We observed (Fig. 2c) a statistically significant effect of pre-adaptation where subjects presented, over the same targets, a bigger biomechanical error during the first block of adaptation with respect to the first block of generalization (NC = 1.72 ± 0.38 for adaptation, 1.45 ± 0.28 for generalization, $p < 0.01$ using Wilcoxon's signed rank test). Finally, to check for a dependency of generalization from the distance to pre-adapted targets, we calculated the extent of generalization for each target as the difference between the average (across repetitions and subjects) NC during the first block of adaptation and the first block of generalization and grouped the targets depending on how many adjacent pre-adapted targets they had during generalization. The smaller amount of generalization was observed for target SW (Fig. 2d) that was the only target that did not have adjacent pre-adapted targets. Targets that presented one adjacent pre-adapted target showed limited generalization. The only target that had both adjacent targets pre-adapted before Ad4 (target N) showed the highest level of generalization.

Adaptation is achieved through the rotation of fixed motor modules. Gentner and colleagues³⁶ have shown that adaptation to visuomotor rotations is fully explained by a rotation (or tuning) of the activation patterns of a fixed set of muscle synergies. Here we demonstrate that the motor module themselves do not change during this kind of adaptation, thus the synergies recorded at baseline can be used to reconstruct the muscular activity recorded during the whole experiment. Similarly to previous works^{36,40}, we found that four muscle synergies, extracted using the non-negative matrix factorization algorithm (NMF)⁴¹ could satisfactorily reconstruct the EMG activity of all subjects during baseline, adaptation and washout (average Variance Accounted For (VAF) across subjects >90%, see Fig. S1 in Supplementary material). This result is consistent with what observed in similar works in literature^{35,36,42}. The synergies extracted from the different subjects were observed to be remarkably similar, with an average normalized dot product at B3 across subjects equal to 0.72 ± 0.08 (Fig. S2).

These four synergies (W1-4) were shown to have distinct functional characteristics and span specific sections of the experimental workspace (Fig. 3a,b). W1 is constituted by the elbow flexors and acts mainly in the lower-left quadrant of the workspace. W2 is constituted by the elbow and shoulder extensors and acts mainly in the upper-right quadrant. W3 is constituted by the muscles commanding shoulder extension and act mainly in the lower-right quadrant. W4 is constituted by muscles involved in shoulder flexion and act mainly in the upper-left quadrant. In our synergistic model of adaptation, we described the adaptive behavior as the modification of the

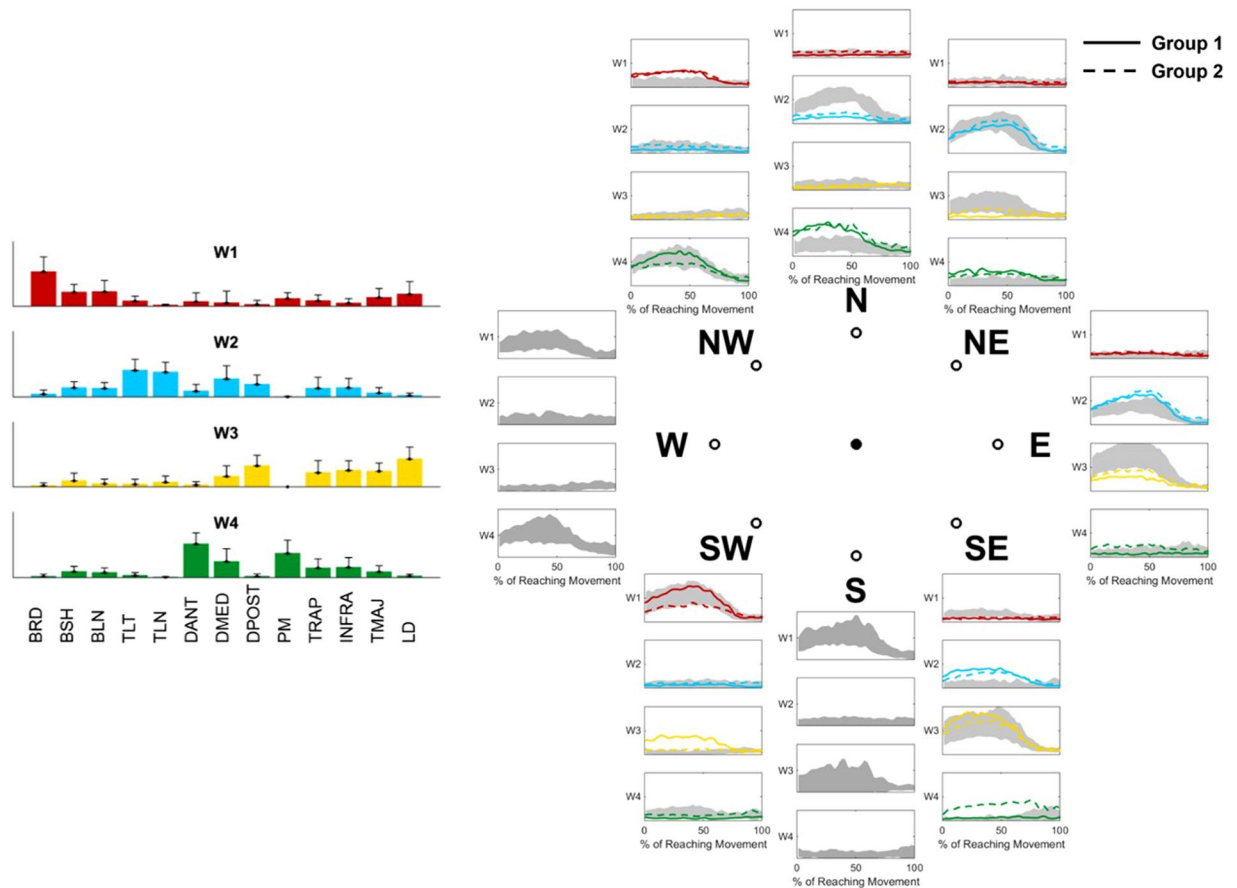


Figure 4. Synergies APs at baseline and final adaptation for each target. Each plot presents the activation patterns (color-coded as their relative synergies on the left of the plot) of each synergy AP for each target. Grey shades represent the average and standard deviation across all subjects at B3, solid lines present the average of the last 5 repetitions of Ad3/Ad6 for Group1, while dashed lines represent the average of the last 5 repetitions of Ad3/Ad6 for Group2.

activation patterns (APs) of a fixed set of reference muscle synergies. The reference synergies were selected as the synergies extracted in the last block of baseline (B3), chosen as the block where subjects were fully habituated to both the task and the movement environment. The choice of fixing the synergy modules as the baseline ones is justified by the high degree of similarity observed, for each subject, between the (unrestricted) synergies extracted at baseline and those extracted at the end of adaptation (dot product equal 0.91 ± 0.06) and washout (dot product equal 0.86 ± 0.10 , Fig. S2).

We then reconstructed the APs relative to the fixed synergies for each block using a modified version of the NMF algorithm⁴⁰. The product between the reference synergies and the block-specific APs yielded average values of VAF > 80% across all subjects and were shown to be significantly higher ($p < 0.01$ for each block, using Mann-Whitney U test and Bonferroni's correction) than VAF values obtained using random reference synergies (Fig. 3c).

Differential paths to adaptation. We then analyzed how the synergies APs converge at the end of adaptation/generalization. Figure 4 shows the average shape of the APs of each target during the last 5 movements of Ad3/Ad6. Since the visual perturbation consists of a 45° CW rotation, in order to adapt subjects need to reach for each target using the motor plan they would use for the adjacent 45° CCW-rotated one. This corresponds to a 45° CW rotation of the synergy APs. As a general observation, the adapted shapes of the APs roughly resemble those observed at baseline for the 45° CCW-rotated target. The average across-targets similarity between the adapted APs and the CCW-rotated ones (calculated as the correlation coefficient between the average of the last five movements at Ad3/Ad6 and the last five movements of the adjacent CCW target at B3) is equal to 0.59 ± 0.15 for adaptation and 0.61 ± 0.06 for generalization, while the similarity between the adapted APs and the baseline ones for the same targets is equal to 0.38 ± 0.17 for adaptation and 0.45 ± 0.13 for generalization. Thus, after adaptation, the APs resemble more those of 45° CCW-rotated targets than the original ones. To further confirm this, we analyzed the similarity between the EMG envelopes recorded at the end of adaptation and generalization (Ad3/Ad6) and the envelopes reconstructed from the synergies weights and APs of the actual and 45° CCW-rotated targets at B3. We found that the envelopes reconstructed from the rotated APs present statistically significant ($p < 0.01$ using Wilcoxon's signed rank test) higher similarity with the adapted recorded envelopes with respect to

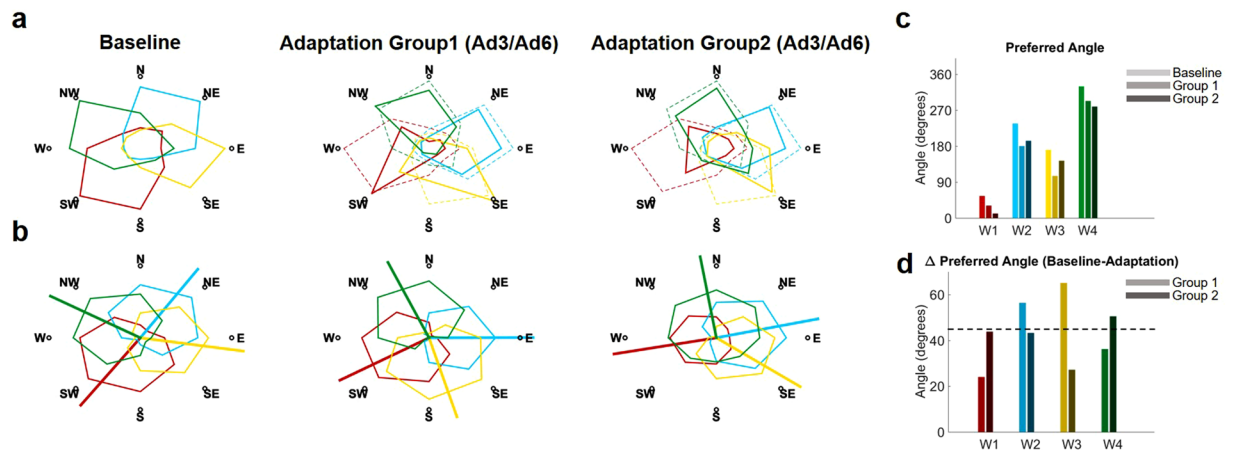


Figure 5. Rotation of the synergies activation patterns and preferred angles. The first row of panel (a) shows the average RMS of the synergies activation patterns (color coded as in Fig. 4) across all targets during Baseline and Full Adaptation for both groups. The Full Adaptation plots were obtained by pooling together the RMSs of the targets at the end of Ad3 (end of first adaptation) and Ad6 (end of generalization). Dashed lines represent the Baseline synergies rotated 45° CW. Both groups present rotations consistent with a 45° CW rotation of the synergies at baseline. The second row (b) presents the same data interpolated using a cosine fit. Outward-pointing lines represent the preferred angles (estimated from the fitting parameters) of each synergy. We observed changes in the preferred angles between Baseline and Full adaptation across the two groups (c). Most preferred angles across the four synergies presented rotations close to the expected 45° (d). The biggest differences in preferred angles after adaptation between the two groups were observed for W1 and W3.

the non-rotated ones (Fig. S3). This analysis has been performed, as cross-validation, by extracting the synergies from Ad3/Ad6 and calculating the similarity between the envelopes reconstructed from these synergy sets and the original (rotated or non-rotated) EMG envelopes recorded at B3.

In Fig. 4 we also notice that the adapted APs differ, for some targets, between the group that trained that target during adaptation and the group that did it during generalization. This behavior can be observed clearly in the APs of W1 for target SW, W3 for targets NE, E and SE and W4 for targets E and SE. This qualitative observation suggests that the synergies APs rotate differently between the two groups.

To confirm upon this point, we calculated and compared the preferred directions of the synergies APs at baseline and after the targets were fully adapted (either during adaptation or generalization) for both groups (Fig. 5). The preferred direction of each AP was calculated from the coefficients of the cosine fitting of the average (across subjects) AP intensity values of all targets and the corresponding target positions^{28,36}. For each group, targets trained during adaptation and generalization were pooled together while calculating the cosine fitting relative to full adaptation. Thus, this analysis does not take into account possible modifications in the APs of the targets trained in Ad1/Ad3 that happen during the Ad4/Ad6 blocks. This analysis can then be considered as a snapshot of the tuned APs relative to each target at their first instance of full adaptation. The comparison between the polar representations of the baseline and adapted APs activation intensities (Fig. 5a) confirm the hypothesis that adaptation is achieved by rotating the APs CW. However, evident differences can be observed between the two groups. The analysis of the preferred angles (Fig. 5b) confirmed this observation. Group1 presented rotations equal to 24°, 56°, 65° and 36° for W1-4, while Group2 presented rotations of 43°, 43°, 27° and 50° (Fig. 5c,d). Interestingly, Group2, that first trained on the target-set spanning the whole workspace (TS2), presented values of final rotations closer to the expected 45°, while Group1 presented over-rotation for two of the synergies (W2 and W3) that cover the workspace of TS1 and under-rotation for the other two (W1 and W4), whose workspace only partially overlaps with the target-set. It appears clear then that the two groups, although presenting the same biomechanical errors at the end of the adaptation/generalization phases of all targets, achieve full adaptation in different ways.

We then analyzed the path to full adaptation for both groups from baseline to washout (Fig. 6). Group1 was able to tune all four synergies by rotating them CW during the exposure to TS1 (Ad1-Ad3), with an emphasis on the synergies mostly spanning the workspace (W2, W3 and W4). During generalization, only small adjustments to the adapted state were sought and regarded exclusively target SW that is the only target that, in our results, did not present a clear generalization behavior. Group2 only tuned three (W1, W2 and W4) of the four synergies during the exposure to TS2, while subsequent adaptation to TS1 was achieved by rotating the previously non-tuned synergy (W3) and only slightly adjusting the rotation of the other ones. Taken all together, these results suggest a dependency of final adaptation on the way in which the synergies are tuned during the initial adaptation period.

Generalization in the synergistic representation of movement. We hypothesized that, if the movement space and thus the adaptation behavior are bound to the workspace spanned by the existing muscle synergies³⁵⁻³⁷, generalization behaviors will also depend on how the synergies are pre-trained. In our experiment we observed patterns of generalization consistent with this hypothesis. The target presenting the highest degree of generalization is target N, which is the only target that, during generalization, had both adjacent targets already

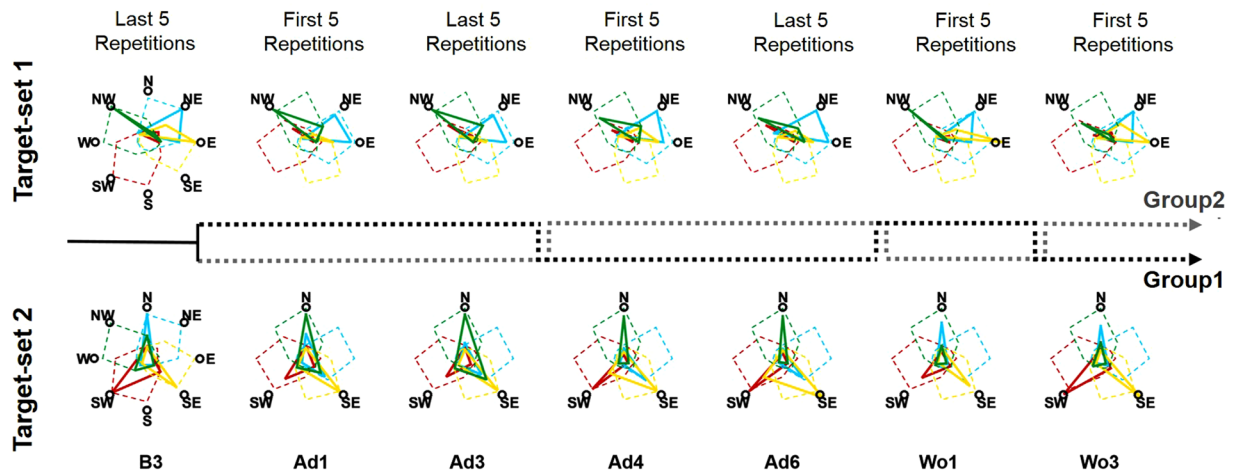


Figure 6. Differential paths to adaptation. The top row presents the changes in AP intensities for TS1 across the different blocks, while the bottom row presents the same results for TS2. For blocks B3, Ad3 and Ad6 the solid lines (color coded as the synergies in Fig. 4) represent the average intensities of the last 5 repetitions for each target, averaged across subjects, while for blocks Ad1, Ad4, Wo1 and Wo3 the solid lines represent the average intensities of the first 5 repetitions for each target, averaged across subjects. For the B3 plots the dashed colored lines represent the workspace spanned by the synergies at baseline as reconstructed using all the targets, while for all the other blocks the dashed colored lines represent the workspace spanned by the synergies at baseline rotated 45° CW. The dashed black and grey lines between the two rows represent the order of repetition for each group. Group1 (black dashed line) performed TS1 during Ad1–Ad3, TS2 during Ad4–Ad6, TS1 during Wo1 and TS2 during Wo3. Group2 (grey dashed line) performed TS2 during Ad1–Ad3, TS1 during Ad4–Ad6, TS2 during Wo1 and TS1 during Wo2.

pre-adapted. Group1, which is the group that experienced target N during generalization (Fig. 7a), presents shapes of APs during the first 5 movements of generalization that are remarkably similar to those observed in the baseline CCW-rotated target. We observed a significant ($p < 0.01$, $\rho = -0.34$) linear correlation between the values of NC and the similarity between the APs at Ad1/Ad4 and the baseline CCW-rotated target (Fig. 7b). We also observed that similarity during generalization is significantly higher than during adaptation (Fig. 7c, $p = 0.03$). These results taken together further confirm that adaptation and generalization to a CW visuomotor rotation depend on a CW tuning of the synergies.

To better understand the reasons behind the different levels of generalization that we observed across the different targets, we analyzed the patterns of generalization with respect to the way in which the synergies are tuned for each target in both groups (Fig. 7d). Target SW, that is the only target that does not present generalization, is adapted by tuning W1 and W3 that are the two synergies presenting the biggest differences in rotation after adaptation between the two groups (Fig. 5d). Target N, on the other hand, is the only target whose adaptation depends on the tuning of synergies W2 and W4, which are the two synergies showing the closest preferred angles between the two groups after adaptation. In Fig. 7e is shown the link between the average APs similarity with the baseline CCW-rotated targets and the difference in preferred angles calculated between the two groups; it is possible to appreciate a trend where targets associated with synergies showing higher differences in the preferred angle after tuning present lower overall similarity. Plotting the average APs similarity with the baseline CCW-rotated targets over the difference in preferred angles calculated between the two groups, it is possible to appreciate a trend where targets associated with synergies showing higher differences in the preferred angle after tuning present lower overall similarity (Fig. 7e). Nevertheless, the differences across the four groups presented in Fig. 7e were not significant ($p = 0.09$ based on Kruskal-Wallis test). These results, although qualitative, suggest that generalization is synergy-dependent and correlates with how similarly the APs tune, during the first adaptation period, towards the optimally tuned preferred angles.

Discussion

Here we have shown that adaptation to visuomotor rotations can be achieved through different rotations of the same set of muscle synergies. The two different final tunings that we observed depend primarily on the initial rotation achieved when adapting to a first sub-set of targets, while subsequent exposures to untrained targets appear to lead only to small adjustments that happen mostly in un-trained or less-trained parts of the workspace. We have also shown that there is an influence of previous synergies tuning on the presence and extent of generalization after pre-adaptation to targets in a shared workspace.

Rotational tunings in muscular and M1 activities have been observed to happen during motor adaptations to visual rotations and force-fields^{43–45}. Those results have been so far extended also to muscle synergies^{35,36}, by demonstrating that simple visuomotor rotations, compatible with the existing synergies workspace, are achieved rapidly through tuning of synergies APs, while more complex adaptations non-describable using the already present synergistic structures may require a slower rewiring of the synergies themselves^{12,35}. The fast

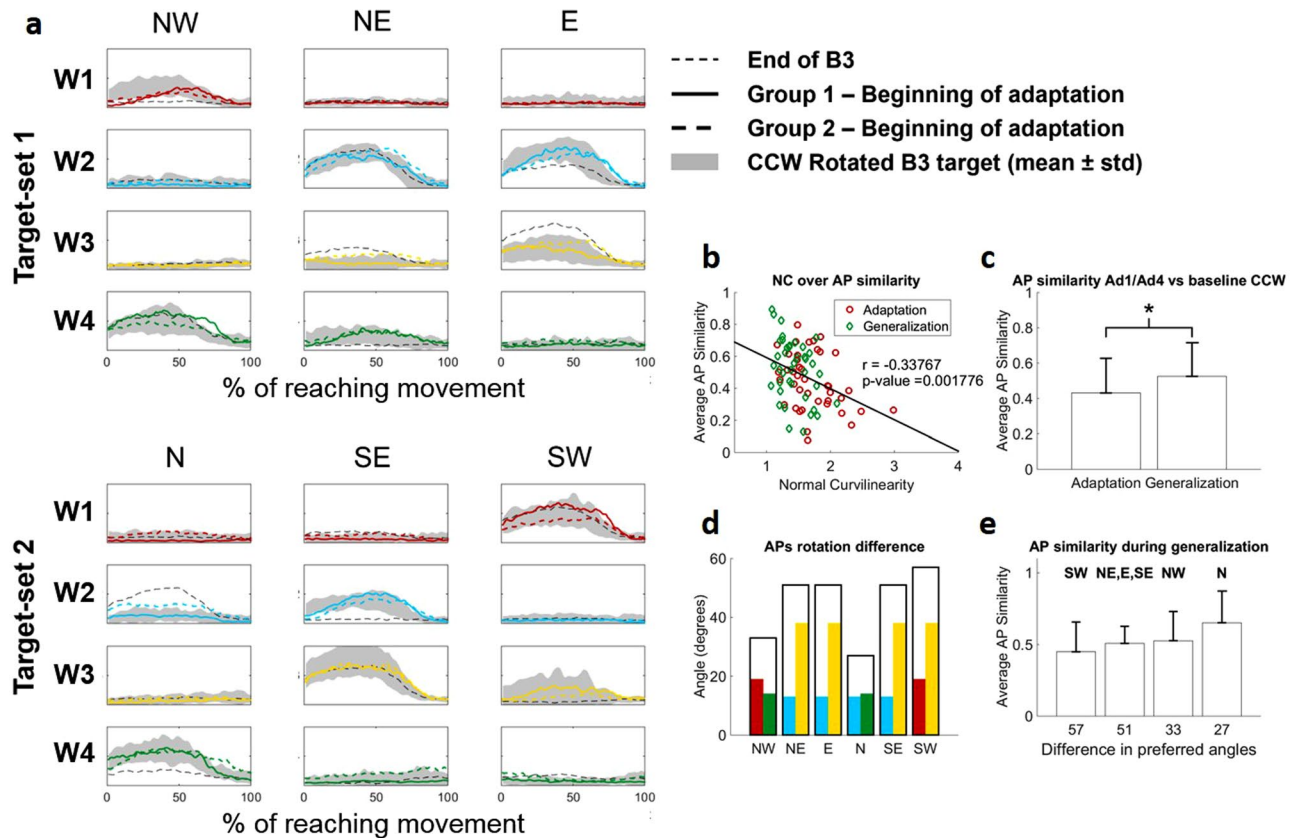


Figure 7. Generalization in the synergies APs. Panel (a) shows the APs of the four synergies (color coded as in Fig. 4) at the beginning of Ad1/Ad4. Solid lines are relative to Group1, while dashed lines are relative to Group2. Shaded areas in each plot represent the activity of each AP in the 45° CCW target at B3 that theoretically represents the goal AP activity for adaptation. The black solid line represents the activity of the APs for each target at the end of B3. For the group/target combination that presents the higher level of generalization (Group1, target N, solid line) the APs at the beginning of generalization are perfectly consistent with the baseline CCW-rotated ones. We observed a significant correlation between the similarity of the APs at the beginning of Ad1/Ad4 with the baseline CCW rotated ones and the values of NC (b) indicating that adaptation and generalization in the biomechanical metric correlates with a 45° rotation of the synergies AP. This result is also confirmed by the fact that the similarity of the APs with the baseline CCW rotated ones is significantly higher for Ad4 with respect to Ad1 (c) ($p = 0.03$, Mann-Whitney U test). We observed a qualitative correlation between the difference in preferred angles at adaptation for the two groups and the level of generalization (d,e). Hollow bars in panel (d) represent, for each target, the sum of the difference in principal angles between the group that adapted the target during adaptation and the one that did it during generalization (as identified in Fig. 5d) for the synergies involved in the reaching to the target (represented by their individual angle difference as colored bars inside the hollow bar). Bars in panel (e) present the average + std values of AP similarity for the targets as grouped by the difference in preferred angles identified in Fig. 7d. The target presenting the higher level of generalization (both in terms of NC and synergies similarity with the baseline rotated ones) is also the target that adapts by tuning the synergies that are more similar between the two groups.

rates of adaptation observed in our results suggest that only the former component of adaptation is at play in our experiment.

We observed, as initially hypothesized, differential paths of APs tuning for the two groups, characterized by under-rotations (W1 for Group1, W3 for Group2), over-rotations (W2 and W3, Group1) and theoretically-optimal rotations (W4 for Group1, W1, W2 and W4 for Group2). Interestingly, most examples of optimally tuned synergies have been observed in Group2, where three of the four synergies appear rotated close to the expected 45°. It is possible that this result is correlated with the fact that Group2 first trains on the target-set (TS2) that spans all the workspace. On the other side, Group1, which was initially trained on a smaller sub-space, presents non-optimal tuning in three of the four synergies. These results, taken together, suggest that optimal synergies tuning is obtained through optimal sampling of the movement space.

A remarkable result herein presented is that it is not enough for a synergy to span the reaching workspace of a given target for it to be tuned in response to a visuomotor rotation. This is exemplified by the behavior that we observed for synergy W3 in Group2. Synergy W3 spans the workspace of targets NE, E and SE, and, when tuned in response to a CW 45° rotation, that of targets E, SE and S (Fig. 5a). TS2 only engages W3 for the adaptation of target SE. Nevertheless, since the activity of W3 is the same between targets SE and E (that is, in this case, the

tuned version of target SE), Group2 does not tune *W3* during the first adaptation period, as confirmed by its non-rotation at Ad4, and instead adapts target SE by tuning *W4* (Figs 4 and 6). Group1, on the other hand, tunes *W3* while adapting for target E, whose goal-target NE presents a completely different AP shape for *W3* and uses the tuned synergy also when adapting to SE during the generalization trials. The only other example of an AP that does not necessarily require tuning for adaptation to a target is, in our experiments, *W2*, when tuned to adapt for target NE. *W2* presents in fact the same activation profile for both NE and its goal-target N. Nevertheless, Group1 still tunes *W2* during the adaptation trial likely because this synergy is also engaged for the adaptation of target E, which requires a modification in its AP. The results on *W3* and *W2* seem to indicate that synergies are tuned only if engaged at the boundaries of their workspace.

The patterns of differential adaptation that we observed suggest that the synergies APs are not the parameters that are directly adapted by the CNS, but rather the tools that are differentially tuned to adapt, while high-level adaptation is likely obtained by updating the sensorimotor transformations mapping the visual targets to the force directions^{36,46}. Then, as different muscular activation patterns can produce the same force⁴⁷, similarly can different combinations of synergies APs, without necessarily invalidating the synergies hypothesis. From our results it appears that muscle synergies constrain the adaptable mapping between the desired motion and the motor commands². Given the sensory prediction error calculated in the forward representation of movements⁴⁸, motor commands are then updated in the synergy-space in a parsimonious way, thus leaving preferably un-altered the synergistic structure (unless changes are necessary³⁵) and the APs that are compatible with the desired force output.

We initially hypothesized that, if adaptation patterns are constrained by the synergistic structural components of the workspace (as our experiment appears to confirm), this likely reflects also on how training on an initial set of targets generalizes on a set of newly experienced ones in the same workspace. In accordance with our hypothesis, the results of our experiment show that the patterns of generalization after pre-adaptation depend on pre-tuning of specific synergies. The target presenting the higher level of generalization is target N, which requires the tuning of synergies *W2* and *W4*. As observed in Fig. 6 both groups are able to engage these two synergies at their boundaries (Group1 while training NW, NE and E; Group2 while training N and SE) in two sub-spaces of identical extension (135°) and rotated of only 45° between them. As a result, the final tuning of those two synergies is similar between the two groups and close to the theoretically ideal rotation (45°). The biggest differences in AP tuning between the two groups are observed in *W3* and, to a smaller extent, *W1*. It is then interesting to notice that all the targets showing limited generalization recruits at least one of these two synergies for its adaptation (Fig. 7d), while target SW, that does not show generalization, recruits both.

Our results are in agreement with previous studies showing that generalization of visuomotor rotations depends on the angular distance between the pre-adapted targets and the new ones^{16,38}. In fact, in the synergy-tuning model of adaptation, pre-training on sub-spaces close to the one that needs to be generalized is likely to lead to the adaptation of one or more of the synergies that are involved in the adaptation of the new movement. This conceptual model could also explain the results showed by Abeele and colleagues³⁹, who found that visual rotations up to 120° present a beneficial effect of pre-adaptation to a 45° smaller rotation, but rotations bigger than 120° did not present a beneficial effect of pre-training. These behaviors may depend, at the synergistic level, on the discrepancy in the workspace covered by the original synergies, the pre-tuned ones and the ones that need to be ultimately tuned. Our results suggest that if the synergy sets involved in all three movements (original, pre-adapted and generalized) fully overlap, generalization is maximized, while as different synergies are recruited (as it is likely for big deviations, as in our 4-synergy space most movement are driven by just two APs that usually span about 160°) generalization is reduced or lost.

As an additional remark, in this work we present an analysis based on the extraction of 4 synergies. Although the interpretation of our results is bound to the shapes and functional characteristics of these 4 synergies, the choice is arbitrary, as arbitrary are all criteria used for order selection in muscle synergy analysis. Nevertheless, ours and previous results in literature^{35,36} suggest that the result we are observing are independent from the number of modules selected during the extraction of muscle synergies.

In conclusion, our results present evidence that the modularity in motor commands as explained by a muscle synergies model influences motor adaptation and its generalization. Considering the rich literature describing visuomotor adaptations, our results present the rationale for considering the functional constraints posed by modular organization of movement in the interpretation of the results of adaptation experiments. The link between muscle synergies, adaptations and, possibly, the mechanisms of motor learning, could have sensible practical validity in the field of neurorehabilitation, where synergistic representation of the impaired and target movements, and of the “modular” path that can be used to translate the former into the latter, could be used to design ad-hoc therapies for patients.

Methods

Experimental setup and Protocol. Fourteen healthy individuals (7 females, age 25.6 ± 1.2) participated in this study. Each individual participated in a single experimental session consisting of a series of isometric reaching tasks performed with their right arm. All the experimental procedures described in the following have been approved by the Ethical Committee of University College Dublin and have been conducted according to the WMA's declaration of Helsinki. All subjects gave written informed consent before participating in this study. During the exercises the subjects sat in a chair with their back straight. Their right forearm was put on a support plan. The hand was strapped to a fixed manipulandum (consisting of a metal cylinder of 4 cm of diameter) attached to a tri-axial load cell (3A120, Interface, UK), while the wrist and forearm were wrapped to the support plan and immobilized using self-adhesive tape. Data from the load cell were sampled at 50 Hz. During all exercises, subjects kept their elbow flexed at 90° and their shoulder horizontally abducted at about 45° (Fig. 1a), so that the manipulandum would be exactly in front of the center of rotation of their shoulder. The elevation of the chair

was controlled so to keep the shoulder abducted at 100°. Subjects sat in front of a screen displaying a virtual scene. The virtual scene consisted of a grey cursor, commanded in real time by the x and y components of the force exerted on the load cell through the manipulandum, a filled circle indicating the center of the exercise space and, depending on the phase of the exercise, a target, represented by a hollow circle. Both the center and target circles had a radius of 1.3 cm. Across all the blocks of the experiment subjects experienced a total of 8 different targets, positioned in a compass-like configuration (Fig. 1b) at a distance of 9.5 centimeters from the center of the screen. The force-to-pixel ratio of the virtual scene was set so that each target was positioned at a distance of 15 N with respect to the center (representing 0 N applied to the load cell) of the scene. The virtual scene and the exercise protocol were controlled using a custom software. The experiment was divided in fourteen different blocks during which subjects were asked to reach for different targets shown on the virtual scene. Subjects were allowed to rest for 1 minute between consecutive blocks.

At the beginning of the experiment subjects performed a Normalization (NM) block. In this block subjects were asked to reach for each one of the eight targets three times and hold the cursor on the target for 5 seconds. In this and all subsequent blocks the targets were presented in a pseudo-random order with the constraint that the same target could not be shown consecutively more than two times. The EMG signals recorded during this block were used to normalize the amplitude of the EMGs for the estimation of muscle synergies. After the NM block, subjects performed three Baseline (B1–B3) blocks. In these blocks subjects were asked to reach for each of the eight targets five times in a random order. In these and all subsequent blocks subjects were asked to complete each reaching movement in less than 1.5 seconds, calculated between the instant in which the cursor exited the central mark circle up to the instant it reached the target hollow circle. Subjects were shown positive feedback for movements performed in less than 1.5 seconds, consisting in the target circle turning green, and negative feedback for movements performed in more than 1.5 seconds, consisting in the target circle turning red. Targets that were performed too slowly were discarded and repeated at the end of the block. After the B1–B3 blocks, subjects performed three Adaptation (Ad1–Ad3) and three Generalization (Ad4–Ad6) blocks. In all these blocks a visual perturbation was applied to the movement of the cursor consisting of a 45° clockwise rotation of the cursor trajectory with respect to its actual one. In each of these blocks subjects performed ten repetitions of three targets randomly presented on the screen. Subjects were divided in two groups (7 individuals each group). Group1 experienced targets NW, NE and E during the Ad1–Ad3 blocks and targets N, SE and SW during the Ad4–Ad6 blocks, while Group2 experienced the target-sets in the inverse order. After the Ad1–Ad6 blocks subjects performed four washout blocks each consisting of ten repetitions of three targets, this time without the visual perturbation. In the first two blocks of Washout (Wo1–Wo2) subjects reached to the targets trained in Ad1–Ad3, while in the second two blocks (Wo3–Wo4) they reached to the targets trained in Ad4–Ad6.

Biomechanical analysis. The data recorded from the load cell was processed and analyzed to characterize the biomechanical patterns of adaptation and generalization of the two groups of subjects. Only the x and y components of the load cell were considered. The continuous load cell data recorded during each block were first low-pass filtered at 10 Hz using a 3rd order Butterworth filter. After filtering, the load cell data of each reaching movement were segmented between the instant in which the cursor exited the central circle and the instant in which it reached the target circle. All segments were then time-scale normalized to 100 samples. We evaluated the adaptation and generalization patterns by calculating the Normal Curvilinearity (NC) of their reaching trajectories. NC was calculated for each length-normalized movement as the ratio between the length of each movement trajectory and the length of the straight line connecting the boundaries of the circles representing the center of the space and the target. A statistical analysis was performed to assess for differences in the average NC values calculated at the beginning of adaptation and generalization of all targets pooled together to assess for differences in NC due to generalization. This analysis was based on Mann-Whitney U test with significance level α set to 0.05.

EMG signal recording and processing. EMG signals were recorded from the following 13 upper limb muscles: Brachiradialis (BRD), Biceps brachii short head (BSH), Biceps brachii long head (BLH), Triceps brachii lateral head (TLT), Triceps brachii long head (TLN), Deltoid Anterior (DANT), Medial (DMED) and Posterior (DPOST) heads, Pectoralis Major (PM), Inferior head of the Trapezius (TRAP), Teres Major (TMAJ) and Latissimus Dorsi (LD). EMG signals were recorded through a Delsys Trigno system (Delsys, US), sampled at 2000 Hz and synchronized with the load cell. All the subsequent analyses were performed in the Matlab environment (2014b, Mathworks, US). EMG signals were filtered in the 20Hz–400Hz band by using a 3rd order digital Butterworth filter. Amplitude envelopes were then obtained by low pass filtering the full wave rectified EMGs with a 3rd order Butterworth filter with a cut-off frequency of 10 Hz. Only the EMG data relative to the center-out phase of the movement, as identified from the biomechanical data, were utilized in the synergies analysis.

Before muscle synergies extraction, all the calculated envelopes underwent an amplitude and time scale normalization procedure. Time scale was normalized by segmenting the EMG data based on the synchronized biomechanical data. Each center-out reaching movement was time-scale normalized by resampling the corresponding envelope on a fixed 100-samples time reference, representative of the percentage of execution of each reaching movement. The EMG envelopes of each subject were amplitude normalized by using the values extracted from the initial normalization block; during the normalization block, each participant reached three times to all the 8 targets, and the peak amplitude of each muscle during each movement was calculated. For each muscle the target yielding its maximal activation was identified. The reference normalization value for each muscle was then established as the average across the three peak values recorded across the repetitions of the target maximizing each muscle's activity during the normalization block.

Muscle synergies extraction. In our main analysis muscle synergies were extracted from each participant at block B3. In an additional analysis (see Figs S1, S2 and S3, Supplementary material) synergies were also

extracted, for each subject, for the data relative to blocks Ad3 and Ad6 pooled together and for the data relative to blocks Wo2 and Wo4 pooled together. The NMF algorithm with multiplicative update rule⁴¹ was applied to the matrix $D_{13 \times (40 \times 100)}$ of the EMG envelopes, containing the time scale and amplitude normalized EMGs from the 40 reaching movements (8 targets \times 5 trials). For each subject, a synergy vectors matrix $W_{13 \times S}$ and a matrix $AP_{S \times (40 \times 100)}$ of the synergy activation patterns was obtained; a number of synergies from 1 to 13 was extracted, and S was defined as the lowest number of synergies able to explain an average (across subjects) fraction of variance higher than 90%. Similarity between different synergy weights (either across or within subjects) was calculated using the normalized dot product (see Supplementary material).

Synergies Activation Patterns reconstruction during motor adaptation using the fixed B3 synergies and statistical validation.

For each subject, the EMG envelopes of all the subsequent adaptation blocks Ad1–Ad6 and washout blocks Wo1–Wo4 were reconstructed by using the set of baseline synergies extracted at B3 from the same subject. This was achieved by using a modified version of the NMF algorithm (namely Nonnegative Reconstruction, NNR)⁴⁰, able to reconstruct the matrix D by letting only the coefficients matrix AP update at every algorithm iteration, while keeping the W matrix fixed. The ability of the B3 synergies to account for the envelopes from all the trials was verified in two separate ways. First, the variance accounted for by the reconstruction (VAF_{REC}) was quantified and statistically compared across trials. In second instance the obtained VAF_{REC} values were statistically compared to those expected from chance. For each subject and each block, 100 random synergy matrixes were obtained by shuffling the muscle components within each synergy, in order to obtain structure-less synergy matrixes $W_{SHUFFLE}$. These matrixes were then used in NNR algorithm and obtain $VAF_{SHUFFLE}$ values from structure-less modules. We then tested for significant differences between VAF obtained from the reference synergies and those obtained from chance for each block. This analysis was based on Mann-Whitney U test with $\alpha = 0.05$ and Bonferroni's correction to take into account the repeated analysis on 11 blocks (from B3 to Wo4), for an effective α of 0.0045.

Calculation of the preferred angles of the synergies APs.

To evaluate the angular tuning of synergies APs, we calculated the preferred angle spanned by each synergy AP in the workspace at both baseline and at full adaptation for all 6 adapted/generalized targets. Preferred angles were calculated from the parameters of a cosine fit²⁸ between the RMS of each synergy and the corresponding target position. Synergies APs were fitted using a linear regression in the form: $AP(\theta) = \beta_0 + \beta_1 \cos(\theta) + \beta_2 \sin(\theta)$. The preferred angle of each synergy was then calculated from the fitting parameters as $\vartheta = \tan^{-1}(\beta_2/\beta_1)$. The preferred angles at baseline were calculated from the RMS of the average (across repetitions and subjects) APs at B3. Preferred angles at final adaptation were calculated by pooling together, for each group, the RMS of the average (across the last 5 repetitions of each target and across subjects) APs at the end of Ad3 and Ad6.

Quantification of AP similarity between current and CW rotated targets.

During the Ad1–Ad6 blocks, each synergy AP_X towards a target X , as obtained from applying the NNR algorithm, was compared with the corresponding average AP_{X-45° towards the 45° CCW-rotated target at B3. Similarity was quantified by calculating the correlation coefficient between AP_X and AP_{X-45° for each target. Specifically, the similarity was calculated between the average AP_{X-45° of the last five repetitions of a given target at B3 and the average AP calculated in either the first or last 5 repetitions of a movement in a certain block. To assess for differences in the final adaptation states (see Results, *Differential paths to adaptation*) the similarities were calculated between B3 and the end of Ad3 and Ad6. To assess for differences in generalization the similarities were calculated between B3 and the beginning of Ad1 and Ad4. In this latter analysis, Wilcoxon's signed rank test was performed to statistically compare AP similarity between targets differently used as adaptation or generalization targets by the two groups. Linear correlation analysis was also used to assess for linear correlation between the similarities calculated between B3 and Ad1/Ad4 and the relative values of NC observed at Ad1/Ad4. Strength and significance of the linear correlation were assessed using Spearman's coefficient. A statistical analysis was employed to assess for differences in the values of similarities between B3 and Ad1/Ad4 depending on the targets grouped by the difference in preferred angles between baseline and adaptation. This analysis was based on Kruskal-Wallis test with $\alpha = 0.05$. In an additional analysis we investigated the similarity between the EMG envelopes recorded at the end of adaptation (Ad3 and Ad6) and those reconstructed from the B3 synergies and the relative AP_X and AP_{X-45° . We also cross-validated this analysis by investigating the similarity between the EMG envelopes recorded at B3 for the normal and rotated targets and those reconstructed from the synergies extracted at Ad3/Ad6. Similarity in this case was calculating using the R^2 metrics (see Fig. S3 Supplementary material).

Data availability. Please contact GS to obtain a copy of the data.

References

- Lackner, J. R. & Dizio, P. Rapid adaptation to Coriolis force perturbations of arm trajectory. *J Neurophysiol* **72**, 299–313, <https://doi.org/10.1152/jn.1994.72.1.299> (1994).
- Shadmehr, R. & Mussa-Ivaldi, F. A. Adaptive representation of dynamics during learning of a motor task. *J Neurosci* **14**, 3208–3224 (1994).
- Wolpert, D. M., Miall, R. C. & Kawato, M. Internal models in the cerebellum. *Trends Cogn Sci* **2**, 338–347 (1998).
- Bhushan, N. & Shadmehr, R. Computational nature of human adaptive control during learning of reaching movements in force fields. *Biol Cybern* **81**, 39–60, <https://doi.org/10.1007/s004220050543> (1999).
- Kawato, M. Internal models for motor control and trajectory planning. *Curr Opin Neurobiol* **9**, 718–727 (1999).
- Wagner, M. J. & Smith, M. A. Shared internal models for feedforward and feedback control. *J Neurosci* **28**, 10663–10673, <https://doi.org/10.1523/JNEUROSCI.5479-07.2008> (2008).

7. Flanagan, J. R. *et al.* Composition and decomposition of internal models in motor learning under altered kinematic and dynamic environments. *J Neurosci* **19**, RC34 (1999).
8. Mussa-Ivaldi, F. A. & Bizzi, E. Motor learning through the combination of primitives. *Philos Trans R Soc Lond B Biol Sci* **355**, 1755–1769, <https://doi.org/10.1098/rstb.2000.0733> (2000).
9. Thoroughman, K. A. & Shadmehr, R. Learning of action through adaptive combination of motor primitives. *Nature* **407**, 742–747 (2000).
10. Donchin, O., Francis, J. T. & Shadmehr, R. Quantifying generalization from trial-by-trial behavior of adaptive systems that learn with basis functions: theory and experiments in human motor control. *J Neurosci* **23**, 9032–9045 (2003).
11. Poggio, T. & Bizzi, E. Generalization in vision and motor control. *Nature* **431**, 768–774, <https://doi.org/10.1038/nature03014> (2004).
12. Sing, G. C., Joiner, W. M., Nanayakkara, T., Braynov, J. B. & Smith, M. A. Primitives for motor adaptation reflect correlated neural tuning to position and velocity. *Neuron* **64**, 575–589, <https://doi.org/10.1016/j.neuron.2009.10.001> (2009).
13. Gandolfo, F., Mussa-Ivaldi, F. A. & Bizzi, E. Motor learning by field approximation. *Proc Natl Acad Sci USA* **93**, 3843–3846 (1996).
14. Goodbody, S. J. & Wolpert, D. M. Temporal and amplitude generalization in motor learning. *J Neurophysiol* **79**, 1825–1838, <https://doi.org/10.1152/jn.1998.79.4.1825> (1998).
15. Krakauer, J. W., Ghilardi, M. F. & Ghez, C. Independent learning of internal models for kinematic and dynamic control of reaching. *Nat Neurosci* **2**, 1026–1031, <https://doi.org/10.1038/14826> (1999).
16. Woolley, D. G., de Rugy, A., Carson, R. G. & Riek, S. Visual target separation determines the extent of generalisation between opposing visuomotor rotations. *Exp Brain Res* **212**, 213–224, <https://doi.org/10.1007/s00221-011-2720-1> (2011).
17. Giszter, S. F., Mussa-Ivaldi, F. A. & Bizzi, E. Convergent force fields organized in the frog's spinal cord. *J Neurosci* **13**, 467–491 (1993).
18. d'Avella, A., Saltiel, P. & Bizzi, E. Combinations of muscle synergies in the construction of a natural motor behavior. *Nat Neurosci* **6**, 300–308, <https://doi.org/10.1038/nn1010> (2003).
19. Cheung, V. C., d'Avella, A. & Bizzi, E. Adjustments of motor pattern for load compensation via modulated activations of muscle synergies during natural behaviors. *J Neurophysiol* **101**, 1235–1257, <https://doi.org/10.1152/jn.01387.2007> (2009).
20. Bizzi, E. & Cheung, V. C. The neural origin of muscle synergies. *Front Comput Neurosci* **7**, 51, <https://doi.org/10.3389/fncom.2013.00051> (2013).
21. Overduin, S. A., d'Avella, A., Carmena, J. M. & Bizzi, E. Microstimulation activates a handful of muscle synergies. *Neuron* **76**, 1071–1077, <https://doi.org/10.1016/j.neuron.2012.10.018> (2012).
22. Overduin, S. A., d'Avella, A., Carmena, J. M. & Bizzi, E. Muscle synergies evoked by microstimulation are preferentially encoded during behavior. *Front Comput Neurosci* **8**, 20, <https://doi.org/10.3389/fncom.2014.00020> (2014).
23. Overduin, S. A., d'Avella, A., Roh, J., Carmena, J. M. & Bizzi, E. Representation of Muscle Synergies in the Primate Brain. *J Neurosci* **35**, 12615–12624, <https://doi.org/10.1523/JNEUROSCI.4302-14.2015> (2015).
24. Saltiel, P., Wyler-Duda, K., D'Avella, A., Tresch, M. C. & Bizzi, E. Muscle synergies encoded within the spinal cord: evidence from focal intraspinal NMDA iontophoresis in the frog. *J Neurophysiol* **85**, 605–619, <https://doi.org/10.1152/jn.2001.85.2.605> (2001).
25. Levine, A. J. *et al.* Identification of a cellular node for motor control pathways. *Nat Neurosci* **17**, 586–593, <https://doi.org/10.1038/nn.3675> (2014).
26. Caggiano, V., Cheung, V. C. & Bizzi, E. An Optogenetic Demonstration of Motor Modularity in the Mammalian Spinal Cord. *Sci Rep* **6**, 35185, <https://doi.org/10.1038/srep35185> (2016).
27. d'Avella, A., Fernandez, L., Portone, A. & Lacquaniti, F. Modulation of phasic and tonic muscle synergies with reaching direction and speed. *J Neurophysiol* **100**, 1433–1454, <https://doi.org/10.1152/jn.01377.2007> (2008).
28. d'Avella, A., Portone, A., Fernandez, L. & Lacquaniti, F. Control of fast-reaching movements by muscle synergy combinations. *J Neurosci* **26**, 7791–7810, <https://doi.org/10.1523/JNEUROSCI.0830-06.2006> (2006).
29. d'Avella, A., Portone, A. & Lacquaniti, F. Superposition and modulation of muscle synergies for reaching in response to a change in target location. *J Neurophysiol* **106**, 2796–2812, <https://doi.org/10.1152/jn.00675.2010> (2011).
30. Ting, L. H. & Macpherson, J. M. A limited set of muscle synergies for force control during a postural task. *J Neurophysiol* **93**, 609–613, <https://doi.org/10.1152/jn.00681.2004> (2005).
31. De Marchis, C., Castronovo, A. M., Bibbo, D., Schmid, M. & Conforto, S. Muscle synergies are consistent when pedaling under different biomechanical demands. *Conf Proc IEEE Eng Med Biol Soc* **2012**, 3308–3311, <https://doi.org/10.1109/EMBC.2012.6346672> (2012).
32. De Marchis, C. *et al.* Feedback of mechanical effectiveness induces adaptations in motor modules during cycling. *Front Comput Neurosci* **7**, 35, <https://doi.org/10.3389/fncom.2013.00035> (2013).
33. Cheung, V. C. *et al.* Stability of muscle synergies for voluntary actions after cortical stroke in humans. *Proc Natl Acad Sci USA* **106**, 19563–19568, <https://doi.org/10.1073/pnas.0910114106> (2009).
34. Cheung, V. C. *et al.* Muscle synergy patterns as physiological markers of motor cortical damage. *Proc Natl Acad Sci USA* **109**, 14652–14656, <https://doi.org/10.1073/pnas.1212056109> (2012).
35. Berger, D. J., Gentner, R., Edmunds, T., Pai, D. K. & d'Avella, A. Differences in adaptation rates after virtual surgeries provide direct evidence for modularity. *J Neurosci* **33**, 12384–12394, <https://doi.org/10.1523/JNEUROSCI.0122-13.2013> (2013).
36. Gentner, R., Edmunds, T., Pai, D. K. & d'Avella, A. Robustness of muscle synergies during visuomotor adaptation. *Front Comput Neurosci* **7**, 120, <https://doi.org/10.3389/fncom.2013.00120> (2013).
37. de Rugy, A., Hinder, M. R., Woolley, D. G. & Carson, R. G. The synergistic organization of muscle recruitment constrains visuomotor adaptation. *J Neurophysiol* **101**, 2263–2269, <https://doi.org/10.1152/jn.90898.2008> (2009).
38. Krakauer, J. W., Pine, Z. M., Ghilardi, M. F. & Ghez, C. Learning of visuomotor transformations for vectorial planning of reaching trajectories. *J Neurosci* **20**, 8916–8924 (2000).
39. Abeele, S. & Bock, O. Sensorimotor adaptation to rotated visual input: different mechanisms for small versus large rotations. *Exp Brain Res* **140**, 407–410, <https://doi.org/10.1007/s002210100846> (2001).
40. Muceli, S., Boye, A. T., d'Avella, A. & Farina, D. Identifying representative synergy matrices for describing muscular activation patterns during multidirectional reaching in the horizontal plane. *J Neurophysiol* **103**, 1532–1542, <https://doi.org/10.1152/jn.00559.2009> (2010).
41. Lee, D. D. & Seung, H. S. Learning the parts of objects by non-negative matrix factorization. *Nature* **401**, 788 (1999).
42. Roh, J., Rymer, W. Z. & Beer, R. F. Robustness of muscle synergies underlying three-dimensional force generation at the hand in healthy humans. *J Neurophysiol* **107**, 2123–2142, <https://doi.org/10.1152/jn.00173.2011> (2012).
43. Li, C. S., Padoa-Schioppa, C. & Bizzi, E. Neuronal correlates of motor performance and motor learning in the primary motor cortex of monkeys adapting to an external force field. *Neuron* **30**, 593–607 (2001).
44. Thoroughman, K. A. & Shadmehr, R. Electromyographic correlates of learning an internal model of reaching movements. *Journal of Neuroscience* **19**, 8573–8588 (1999).
45. Wise, S. P., Moody, S. L., Blomstrom, K. J. & Mitz, A. R. Changes in motor cortical activity during visuomotor adaptation. *Exp Brain Res* **121**, 285–299 (1998).
46. Shadmehr, R. & Krakauer, J. W. A computational neuroanatomy for motor control. *Exp Brain Res* **185**, 359–381, <https://doi.org/10.1007/s00221-008-1280-5> (2008).
47. Kutch, J. J. & Valero-Cuevas, F. J. Challenges and new approaches to proving the existence of muscle synergies of neural origin. *PLoS Comput Biol* **8**, e1002434, <https://doi.org/10.1371/journal.pcbi.1002434> (2012).
48. Shadmehr, R., Smith, M. A. & Krakauer, J. W. Error correction, sensory prediction, and adaptation in motor control. *Annu Rev Neurosci* **33**, 89–108, <https://doi.org/10.1146/annurev-neuro-060909-153135> (2010).

Acknowledgements

This study was partially funded by the UCD Seed Grant #SF1303.

Author Contributions

G.S. conceived the study; G.S., C.D.M., J.D.S. and S.C. designed the study protocol; G.S., J.D.S. and M.Z. set up and executed the experiments; G.S., C.D.M. and J.D.S. analyzed the data; G.S. and C.D.M. drafted the manuscript; J.D.S., M.Z. and S.C. reviewed the draft.

Additional Information

Supplementary information accompanies this paper at <https://doi.org/10.1038/s41598-018-31174-2>.

Competing Interests: The authors declare no competing interests.

Publisher's note: Springer Nature remains neutral with regard to jurisdictional claims in published maps and institutional affiliations.



Open Access This article is licensed under a Creative Commons Attribution 4.0 International License, which permits use, sharing, adaptation, distribution and reproduction in any medium or format, as long as you give appropriate credit to the original author(s) and the source, provide a link to the Creative Commons license, and indicate if changes were made. The images or other third party material in this article are included in the article's Creative Commons license, unless indicated otherwise in a credit line to the material. If material is not included in the article's Creative Commons license and your intended use is not permitted by statutory regulation or exceeds the permitted use, you will need to obtain permission directly from the copyright holder. To view a copy of this license, visit <http://creativecommons.org/licenses/by/4.0/>.

© The Author(s) 2018